

Corrigendum

Interchangeable functions of *Arabidopsis* PIROGI and the human WAVE complex subunit SRA1 during leaf epidermal development

Dipanwita Basu, Salah El-Din El-Assal, Jie Le, Eileen Mallery and Daniel B. Szymanski *Development* **131**, 4345-4355.

In this article, the authors reported that complementation tests between *pirogi* and *klunker* plants proved that the two genes were distinct. They have subsequently learned that the *klunker* stocks were mislabeled, and that *KLUNKER* and *PIROGI* correspond to the same gene and encode a SRA1 homologue.

The authors apologise to readers for this mistake and for any confusion caused.

Interchangeable functions of *Arabidopsis* PIROGI and the human WAVE complex subunit SRA1 during leaf epidermal development

Dipanwita Basu¹, Salah El-Din El-Assal¹, Jie Le¹, Eileen L. Mallery¹ and Daniel B. Szymanski^{1,2,*}

¹Agronomy Department, Purdue University, Lilly Hall, 915 West State Street, West Lafayette, IN 47907-2054, USA

²Purdue Motility Group, Purdue University, Lilly Hall, 915 West State Street, West Lafayette, IN 47907-2054, USA

*Author for correspondence (e-mail: dszyman@purdue.edu)

Accepted 14 June 2004

Development 131, 4345-4355
Published by The Company of Biologists 2004
doi:10.1242/dev.01307

Summary

The WAVE complex is an essential regulator of actin-related protein (ARP) 2/3-dependent actin filament nucleation and cell shape change in migrating cells. Although the composition of the WAVE complex is well characterized, the cellular mechanisms that control its activity and localization are not well known. The ‘distorted group’ defines a set of *Arabidopsis* genes that are required to remodel the actin cytoskeleton and maintain the polarized elongation of branched, hair-like cells termed trichomes. Several loci within this group encode homologs of ARP2/3 subunits. In addition to trichome distortion, ARP2/3 subunit mutants have reduced shoot fresh weight and widespread defects in epidermal cell-cell adhesion. The precise cellular function of plant ARP2/3, and the means by which it is regulated, is not known. In this paper, we report that the ‘distorted group’ gene *PIROGI* encodes a homolog of the WAVE complex subunit SRA1. The similar

cell shape and actin phenotypes of *pir* and ARP2/3 complex subunit mutants suggest that *PIROGI* positively regulates ARP2/3. *PIROGI* directly interacts with the small GTPase ATROP2 with isoform specificity and with selectivity for active forms of the protein. *PIROGI* shares only 30% amino acid identity with its human homolog. However, both WAVE subunit homologs are functionally interchangeable and display identical physical interactions with RHO family GTPases and the *Arabidopsis* homolog of the WAVE complex subunit NAP125. These results demonstrate the utility of the ‘distorted group’ mutants to study ARP2/3 complex functions from signaling input to cell shape output.

Supplemental data available online

Key words: Trichome, WAVE, ARP2/3, SRA1, PIR121

Introduction

Trichomes or hairs are present on the surface of most land plants (Johnson, 1975). Although their shapes vary wildly, and are often a useful morphological characteristic with which to distinguish different species, trichomes of a specific type execute fixed morphogenetic programs and acquire very similar shapes. This differs greatly from motile animal cell types that migrate and dynamically reorganize their shape in response to morphogenetic gradients. In plant cells, localized regions of cell expansion are defined by the mechanical properties of the cell wall, such as the location and orientation of cellulose microfibrils, and by the regulated positioning of organelles and vesicles in the cytoplasm. In general, the orientation of cortical microtubules and cellulose microfibrils are related, and actin filaments play a more prominent role in organelle positioning and intracellular transport (Mathur and Hulskamp, 2002). Despite their differing growth strategies, plants, protists and humans employ many of the same cytoskeletal proteins (Assaad, 2001; Staiger and Hussey, 2003). An important challenge in plant development and biotechnology is to better understand how plants generate and use particular cytoskeleton arrays to control the physical properties of cells. The ‘distorted group’ is a useful collection of mutants to determine the role of ARP2/3 subunits and actin during morphogenesis (El-Assal et al., 2004a; Le et al., 2003;

Li et al., 2003; Mathur et al., 2003a; Mathur et al., 2003b). In this paper, we show that the ‘distorted group’ gene *PIROGI* (*PIR*) encodes a WAVE complex subunit homolog that positively regulates ARP2/3.

Arabidopsis leaf trichomes are unicellular structures that have highly constrained and sequential requirements for the microtubule and actin filament cytoskeletons (Beilstein and Szymanski, 2003). Unlike tip-growing root hairs (Baluska et al., 2000), the earliest phases of polarized trichome outgrowth, the initiation of stalk (stage 2) and branch (stage 3) buds, require an intact microtubule cytoskeleton (Mathur et al., 1999; Szymanski et al., 1999). Following branch initiation, microtubules remain important (Szymanski, 2001), but the refinement of the branch tip from a hemispherical dome to a fine point (stage 4) defines the first detectable requirement for an intact actin-cytoskeleton (Szymanski et al., 1999). Mutations in ARP2/3 subunit genes block this morphological transition, and either disorganization of cytoplasmic actin filaments and/or bundles (Szymanski et al., 1999; El-Assal et al., 2004a; Le et al., 2003) or increased bundling of actin filaments (Li et al., 2003; Mathur et al., 2003a; Mathur et al., 2003b) is believed to cause cell swelling and reduced branch elongation.

ARP2/3 is a seven protein complex that binds to the sides of existing actin filaments, and nucleates ‘daughter’ actin

filaments (Amann and Pollard, 2001; Blanchoin et al., 2000). ARP2/3, along with additional actin-binding proteins, can generate dendritic actin networks or highly organized bundles (Svitkina et al., 2003; Vignjevic et al., 2003) that drive plasma membrane protrusion and organelle motility (Pollard and Beltzner, 2002; Schafer, 2002). In yeasts (Winter et al., 1999), flies (Stevenson et al., 2002) and worms (Sawa et al., 2003), ARP2/3 subunit mutations cause severe developmental defects and lethality. *Arabidopsis* ARP2/3 subunit genes are expressed ubiquitously, and plants that carry strong loss-of-function mutations in ARP2/3 subunits have a reduced fresh weight and widespread cell-cell adhesion defects in the shoot (El-Assal et al., 2004a; Le et al., 2003; Li et al., 2003; Mathur et al., 2003a; Mathur et al., 2003b). However, ARP2/3 subunit mutants are viable and overall plant architecture is not affected.

The actin filament nucleation activity of ARP2/3 requires trans-activators such as the WASP (Wiscott-Aldrich syndrome protein)/WAVE (WASP family VERPROLIN-homologous protein) family members (Welch and Mullins, 2002). WAVE directly interacts with the ARP2/3 complex (Machesky and Insall, 1998) and potently enhances the actin filament nucleation activity of the complex (Machesky et al., 1999). The activity of WASP is regulated by relief of autoinhibition (Rohatgi et al., 2000). WAVE is an intrinsically active ARP2/3 activator, and the primary function of the pentameric WAVE complex is to regulate the activity of WAVE (Eden et al., 2002). Although the biochemical details of how the WAVE complex regulates ARP2/3-dependent actin filament nucleation are unresolved (Blagg and Insall, 2004), recent data from several laboratories indicate that the complex controls the stability and/or localization of the WAVE subunit (Blagg et al., 2003; Innocenti et al., 2004; Kunda et al., 2003; Steffen et al., 2004). *Arabidopsis* does not have an obvious ortholog of WASP or WAVE, but WAVE-like activity in *Arabidopsis* is expected given the presence of SRA1-, NAP125- and HSPC300-like genes in *Arabidopsis*.

We provide strong evidence that *PIR* encodes a homolog of the WAVE complex subunit that has been named SPECIFICALLY RAC1-ASSOCIATED (SRA1) (Kobayashi et al., 1998) or *PIR121* (*p53-121F-induced*) (Saller et al., 1999). Both names are used in the literature, and for simplicity in this paper we will refer to the non-plant homologs collectively as SRA1. SRA1 assembles into the WAVE complex via a direct interaction with the NAP125 subunit (Gautreau et al., 2004; Innocenti et al., 2004). SRA1 directly binds to active Rac1 (Kobayashi et al., 1998), and imparts Rac1 responsiveness to the WAVE complex. SRA1 is required for lamellipodia formation in cultured animal cells (Kunda et al., 2003; Rogers et al., 2003), and in vitro activation of Rac1 signaling can cause the relocalization of the fully assembled WAVE complex to the plasma membrane (Steffen et al., 2004).

The 'distorted group' of trichome mutants provides a useful genetic system with which to study a pathway of functions from SRA1 activation to ARP2/3-dependent morphogenesis in vivo. *PIR* encodes a homolog of the WAVE complex subunit SRA1. *PIR* appears to positively regulate ARP2/3, because loss of function mutations in *PIR* and ARP2/3 subunits cause a similar array of cell shape and actin cytoskeleton phenotypes. *PIR* is 30% identical to human SRA1, yet in transformation and *pir* rescue experiments, the human and plant proteins are functionally interchangeable. Despite the high degree of amino

acid sequence divergence between the plant and human SRA1 homologs, their cross-kingdom interactions with RHO GTPases and the *Arabidopsis* homolog of NAP125 (ATNAP125) were indistinguishable.

Materials and methods

Plant strains, growth conditions and plant measurements

For all experiments, Col-0 is the wild-type and all alleles were backcrossed into this background at least five times prior to use. *pir-1* (Col-0) and *pir-2* (Col-0) are untagged T-DNA alleles found in a visual screen of T-DNA insertion seed pools obtained from the *Arabidopsis* stock center. *pir-3* (Col) is a fast neutron-induced allele isolated from an M₂ population (Lehle seeds, Round Rock, TX). *pir-5* was recovered from an EMS-mutagenized M₂ Col-0 population that we generated using a standard mutagenesis protocol. *pir* alleles were sequenced as described previously (El-Assal et al., 2004a). The PIR sequencing templates and primer sequences are listed in Fig. S2 at <http://dev.biologists.org/cgi/content/full/131/17/4345/DC1>. SEM, localization and plant growth measurement experiments employed plants grown on 1/2× MS media with or without 1% sucrose at 25°C with constant illumination. For fresh weight measurement, soil-grown segregating *pir* populations were analyzed as described previously (Le et al., 2003). For measuring gap frequency plants were grown in vitro on 1/2× MS with 1% sucrose. Gaps were counted in 540×390 μm boxes that were overlaid on SEM images of the apical one-third of the 12 days after germination (DAG) cotyledons. This region was chosen in order to restrict our analyses to relatively synchronized fully expanded cells. Gaps from three non-overlapping boxes were counted for each cotyledon, and at least three cotyledons were measured for each genotype. Trichome branch lengths were measured from SEM of stage 6 trichomes and ImageJ software version 1.3. The measured trichomes had three branches that were approximately parallel to the image plane.

Plasmid construction

To create a full length *PIR* clone, 3849 bp of *PIR*-coding region was amplified from pATPOP140 (a gift from C. Staiger) and cloned into Gateway™ vector, pENTR/D/TOPO (pEN) (Invitrogen, Carlsbad, CA) to generate pEN-*PIR*. To generate a full-length human cDNA, 3762 bp of human *SRA1* was amplified by PCR from a full-length cDNA (GenBank Accession Number AB032994). The PCR product was cloned into pEN vector to generate pEN-HSPIR. These and all other PCR-generated clones were sequenced on both strands prior to use. The *Arabidopsis* and human pEN clones were recombined into yeast two-hybrid Gal4 DNA-binding (bait) vector pDEST32 to generate pDS32PIR and pDS32HSPIR, respectively. pEN-*PIR* and pEN-HSPIR were also recombined into the Gateway™ compatible binary vector pGWB2 (a gift from T. Nagawa, Shiman University, Japan), to generate pB2PIR and pB2HSPIR, respectively. pB2PIR and pB2HSPIR were transformed in Col and *pir-3* backgrounds using floral dip protocol (Clough and Bent, 1998). The 4193 bp of *ATNAP125* and 3387 bp of Human *NAP125* were amplified from full-length cDNA (GenBank Accession Numbers AV554904 and AB011159, respectively) and cloned into pEN generating pEN-ATNAP and pEN-HSNAP, respectively. These *Arabidopsis* and human *NAP125* clones were then recombined into the Gateway™ yeast two-hybrid GAL4-activation domain (prey) vector pDEST22 to generate pDS22NAP and pDS22HSNAP, respectively. For protein expression in *E. coli*, pEN-NAP was recombined to Gateway™ N-terminal 6×-His-tag destination vector pDEST17 to generate pDS17NAP. The coding regions of ATROP2 and ATROP8 were PCR amplified from pGEX-ROP2 and pGEX-ROP8, while coding regions of HsRac1 and HsCdc42 were amplified from pGEX-Rac1hs and pGEX-Cdc42hs, respectively. These PCR products were cloned into pEN to generate pEN-ROP2, pEN-ROP8, pEN-HSRAC1 and pEN-

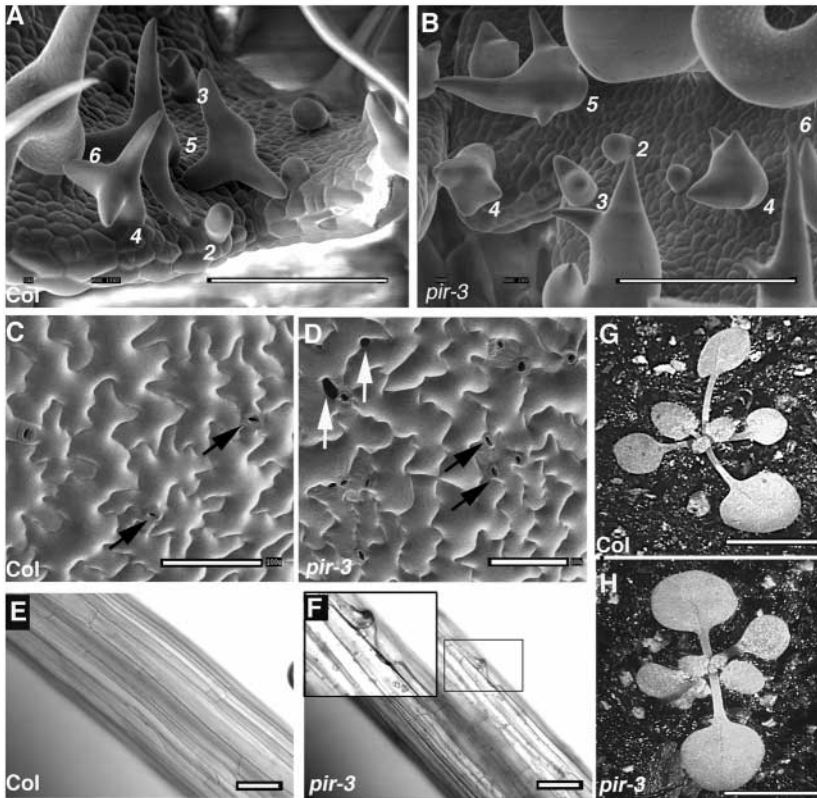


Fig. 1. Epidermal phenotypes of *pir* trichomes, cotyledon pavement cells and hypocotyls. (A) SEM of developing trichomes on the upper surface of developing wild-type leaves. (B) SEM of developing trichomes on the upper surface of developing *pir-3* leaves. (C) SEM of upper surface of 12 DAG (days after germination) wild-type cotyledon pavement cells. (D) SEM of upper surface of 12 DAG *pir-3* cotyledon pavement cells. (E) Hypocotyl of dark-grown wild-type seedlings. (F) Hypocotyl of dark-grown *pir-3* seedlings (boxed area is enlarged in the inset, which shows a higher magnification view of the non-adherent cell). (G) Wild-type plant (15 DAG). (H) *pir-3* plant (15 DAG). Numbers in A and B are positioned in the lower right region of a trichome to indicate the developmental stage. White arrows indicate the gaps between adjacent pavement cells and black arrows indicate stomatal pores in C,D. Scale bars: 100 μ m in A-F; 1 cm in G,H.

HSCDC42. To generate yeast two-hybrid constructs, pEN-ROP2, pEN-ROP8, pEN-HSRAC1 and pEN-HSCDC42 were recombined into pDS22 to generate pDS22ROP2, pDS22ROP8, pDS22HsRAC1 and pDS22HsCDC42, respectively. Site-directed mutagenesis was carried out on pEN-ROP2 and pEN-ROP8 using the Quick-change Site-directed mutagenesis kit (Stratagene, La Jolla, CA) to generate the clones pEN-ROP2G15V, pEN-ROP2T20N, pEN-ROP2D121A, pEN-ROP8G23V, pEN-ROP8T29N and pEN-ROP8D133A. The corresponding yeast two-hybrid plasmids were constructed into pDS22 to generate pDS22ROP2G15V, pDS22ROP2T20N, pDS22ROP2D121A, pDS22ROP8G23V, pDS22ROP8T29N and pDS22ROP8D133A. The PCR primers used for plasmid constructions were named according to the name of the final plasmid produced and are listed in Fig. S4 at <http://dev.biologists.org/cgi/content/full/131/17/4345/DC1>.

Protein-protein interaction assays

For yeast two-hybrid assays pairs of bait and prey plasmids defined in the figures were co-transformed into the *S. cerevisiae* strain Y190 using the lithium acetate method. The transformants were selected on Leu-Trp⁻ medium. Two-hybrid interaction was determined by colony formation on Leu-Trp-His⁻ medium using the *HIS3* reporter gene. For each two-hybrid plasmid, liquid β -galactosidase assays were carried out in triplicate from three independent colonies using standard protocols (Ausubel et al., 1994). For pull-down assays, full-length PIR was expressed as an N-terminal GST fusion protein. pGEX-ATPOP140 (PIR) was transformed into *E. coli* RossettaTM (DE3) strain (Novagen, Madison, WI), induced at OD₆₀₀=0.6–0.8 and then grown at 15°C for 40 hours. Soluble protein was purified using GST beads (Sigma, Steinheim, Germany) using standard protocols. To produce full-length ATNAP125 protein, pDS17NAP construct was transformed in *E. coli* RossettaTM (DE3) strain and induced with 100 μ M IPTG at OD₆₀₀=0.6–0.7 and grown for 4 hours at 37°C. Soluble HIS-ATNAP125 (GRL) protein was purified with Ni²⁺ beads (Novagen,

Madison, WI) using standard protocols. Protein concentrations were determined using the Bradford method. Bead bound GST-PIR (40 nM) was mixed with 100 nM of HIS-ATNAP125 in binding buffer containing 50 mM HEPES/KOH (pH 7.6), 20 mM KCl and 5 mM MgCl₂. Binding reactions were incubated at 4°C for 2 hours. Total, bead-bound and unbound fractions were separated by SDS-PAGE, and transferred to nitrocellulose membranes. HIS-ATNAP125 was detected with polyclonal anti-NAP125 rabbit antibody (1:1,000), and blots were quantitated using densitometry. Anti-NAP125 peptide antibodies were

made in rabbits using amino acids 2–14 (CANSRQYYPSQDES) and 1328–1340 (CSRSGPISYKQHN) of ATNAP125 as antigens. As a control for nonspecific binding of GST-PIR to large HIS-tagged proteins, 40 nM bead-bound GST-PIR was mixed with 120 nM of HIS-AT3G and analyzed as above. HIS-AT3G was detected with a rabbit polyclonal antibody.

F-actin localization and quantitation

Whole-mounted seedlings were fixed at room temperature and processed for F-actin localization and image processing as previously described (Le et al., 2003).

Results

A stage 4 *pir* trichome has the plump appearance of well-stuffed pirogi. In a large-scale screen for distorted mutants we isolated four *pir* alleles. Like all known distorted group mutants, each *pir* allele caused a trichome swelling phenotype that appeared following branch initiation (stage 3) (Fig. 1B). In F₂ populations, recessive *pir-1*, *pir-2*, *pir-3* and *pir-5* alleles segregated close to the expected 3 (wild type): 1 (mutant; for all alleles: $\chi^2 < 1.34$, $P > 0.1$) ratio. Stage 4 is defined as the stage of trichome growth during which the hemispherical apical dome of the elongating branch transitions to a more pointed morphology (Fig. 1A). 36% ($n=25$) of *pir* stage 4 trichomes had a stalk or branch diameter that exceeded 30 μ m, an extent of swelling that was similar to *distorted1* [*dis1* (*arp3*)] and *distorted2* [*dis2* (*arpc2*)] (El-Assal et al., 2004a; Le et al., 2003). Mature *pir* trichomes were swollen and twisted to different degrees, but displayed a consistent reduction in branch length (Table 1). The mean lengths of branches 2 and 3 in *pir* trichomes were significantly less than the wild-type.

Fig. 2. *PIR* encodes a homolog of human *SRA1*. Physical map of the *PIR* gene, mutant alleles and rescue of the mutant phenotype by overexpression. (A) The region of chromosome 5 that contains the *PIR* locus. Boxes indicate the position of molecular markers and the oval represents the *PIR*-containing BAC (T4C15). The measured recombination frequency for several markers in the mapping interval is given. (B) Physical structure of the *PIR* locus. The position of exons and introns are indicated by black rectangles and lines, respectively. The 5'-UTR and 3'-UTR are indicated by white rectangles. The location and nature of the *pir-1*, *pir-2*, *pir-3*, *pir-5* and *pir-T1* mutations are labeled. The location of the AT-AC intron is labeled. The 5'-UTR and 3'UTR sequences were derived from RIKEN clone RAFL04-10-J11 (GenBank Accession Numbers AV82143 and AV781909, respectively). (C) Overexpression of *PIR* rescues *pir-3* trichome phenotype. (Left) Col mature trichome; (middle) *pir-3* mature trichome; (right) mature trichome on a *pir-3* plant that harbors a *PIR* overexpression construct.

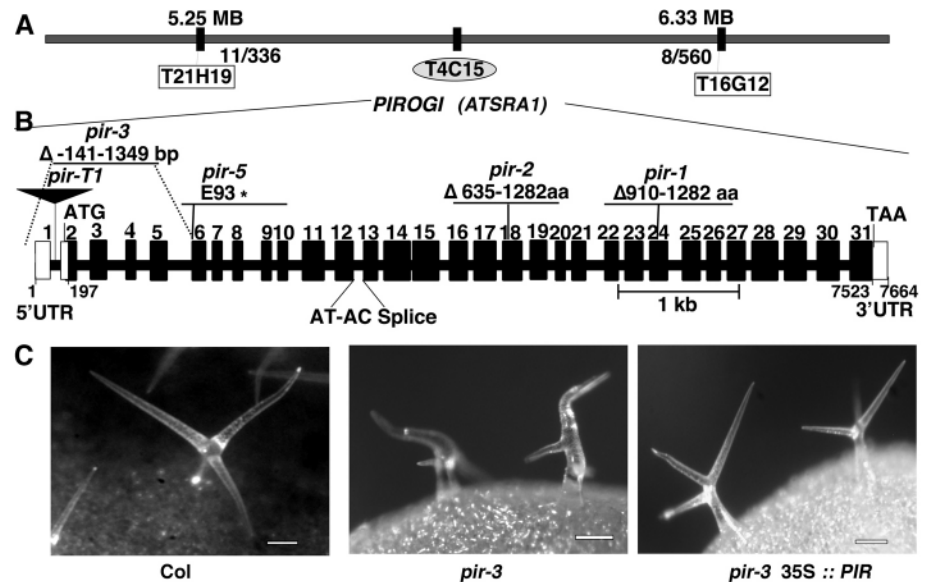


Table 1. Quantification of *pir* trichome branch length, cell adhesion and hypocotyl elongation phenotypes

	Trichome branch length*			Gaps/mm ² †	Hypocotyl length (cm)‡
	Branch 1 (μm)	Branch 2 (μm)	Branch 3 (μm)		
Col	189.8±22.6§ (n=12)	165.9±16.0 (n=12)	119.8±30.5 (n=12)	0±0 (n=3)	1.6±0.11 (n=10)
<i>pir-3</i>	90.9±39.5 (n=12)	49.7±19.5 (n=12)	25.9±11.5 (n=12)	30±9 (n=3)	0.8±0.08 (n=10)
<i>dis2-1</i>	47.4±27.8 (n=12)	27.7±12.9 (n=12)	18.9±8.4 (n=12)	9±8 (n=3)	0.7±0.08 (n=10)

*Length measured from the base to tip along the midline.
†Gaps are defined as two adjacent pavement cells with a clear region of non-adherence.
‡Hypocotyl length of dark grown seedlings was measured at 7 days after germination.
§All measurements are expressed as mean±s.d.

The lengths of all three *dis2* (*arpc2*) branches were significantly less than the wild type.

Wild-type and *pir* cotyledon pavement cells were highly lobed (Fig. 1C,D). *pir* cotyledon pavement cells, like those of *dis2* (*arpc2*) had obvious gaps between adjacent cells (Fig. 1D, Table 1). In our hands, the cell-cell adhesion defect of *dis1* (*arp3*), *dis2* (*arpc2*), *pir* and *gnarled* (*grl*) cotyledon pavement cells is the most consistent pavement cell phenotype, and a reduction in pavement cell lobe formation is apparent in the fraction of cotyledons with the most severe adhesion defects. The relationships between cell-cell adhesion, patchy cell division in the epidermis of true leaves and pavement cell lobing are not resolved in the ARP2/3 subunit mutants. Epidermal cell-cell adhesion was also abnormal in the hypocotyl (Fig. 1F). *pir* dark-grown hypocotyls, like those of *dis2* (*arpc2*), had a reduced mean length (Table 1). *pir* plants had a normal overall architecture (Fig. 1H); however, in segregating populations, each of the four *pir* alleles reduced shoot fresh weight by ~30% relative to segregating wild-type controls. Using the cotyledon as a model, we have not detected clear reductions in organ size, cell size or cell number in *pir* or *dis2* (data not shown).

We were particularly interested in cloning *PIR* because it mapped to an interval on chromosome 5 that did not contain an

ARP2/3 subunit-like gene, and therefore could correspond to a gene with regulatory functions. *PIR* mapped near *KLUNKER* (Schwab et al., 2003), but reciprocal complementation tests proved that *PIR* and *KLUNKER* were different genes. The mapping interval did contain one gene, *ATSRA1* (AT5G18410), which shared a high degree of amino acid sequence identity with the SRA1 subunit of the WAVE complex (Fig. 2A). To determine if *PIR* corresponded to this gene, we assayed the trichome phenotype of plants that were homozygous for the SALK_106757 T-DNA insertion (Alonso et al., 2003). The insertion was located in the first intron of the 5' UTR of *ATSRA1* (Fig. 2B), and lines that were homozygous for the insertion displayed a clear distorted trichome phenotype. Complementation tests indicated that SALK_106757 was a *pir* allele. To confirm the identity of *PIR*, we sequenced the *ATSRA1* gene in each of the four *pir* backgrounds. In each case we found point mutations and deletions that affected *ATSRA1* coding (Fig. 2B, Fig. S1 at <http://dev.biologists.org/cgi/content/full/131/17/4345/DC1>). The *pir-3* fast neutron allele was a null because we failed to detect an *ATSRA1* transcript after two successive rounds of RT-PCR. The *pir-3* RNA sample was intact because the control gene *GAPC* was detected easily in both rounds of RT-PCR (data not shown). As final proof of gene identity, we transformed *pir-3* plants with

a transgene that used the viral 35S promoter to overexpress the full-length *PIR* cDNA. All 12 primary transformants had trichome shape (Fig. 2C) and cotyledon pavement cell-adhesion phenotypes (data not shown) that were indistinguishable from the wild type. For the rest of this manuscript we will refer to *ATSRA1* as *PIR*.

Comparison of the *PIR* genomic sequence and a full-length *PIR* cDNA identified 31 exons that spanned 7664 bp of genomic DNA. Our experimentally determined cDNA sequence (GenBank Accession Number AY662957) differed from the predicted mRNA (GenBank Accession Number NP_197342) at five splice sites. In one interesting splicing discrepancy the experimentally determined mRNA used an AT-AC splice donor-acceptor pair to process intron 12 (Fig. 2B). The accuracy of the *PIR* cDNA sequence was confirmed by sequencing an independent RT-PCR product that spanned the AT-AC splice. We also analyzed combinations of RT-PCR reactions from several flanking exons, and failed to detect alternative splicing (data not shown). AT-AC splicing occurs in *Arabidopsis* (Wu et al., 1996), but the functional significance of this rarely observed splicing mechanism is not known. *PIR* encoded a predicted polypeptide of 140 kDa that shared ~30% identity along its entire length with several SRA1 homologs (Supplemental data S1). The *pir-1*, *pir-2* and *pir-5* alleles encoded progressively severe C-terminal truncations of PIR (see Fig. S1 at <http://dev.biologists.org/cgi/content/full/131/17/4345/DC1>). However, the reductions in trichome branch length, hypocotyl elongation and fresh weight for each *pir* allele were not significantly different (data not shown).

Based on the animal literature, *Arabidopsis PIR* is expected to function as a regulator of the ARP2/3 complex. As an initial test of this idea, we wanted to determine if *PIR*, *ATNAP125* and ARP2/3 subunit-like genes had similar levels and patterns of gene expression. Homologs of each of the seven ARP2/3 subunits share a similar level of expression throughout the plant, with some differences among subunit-like genes such as *DIS2* (*ARPC2*) and *ATARPC4*, in their relative expression levels in leaves and stems (El-Assal et al., 2004a; Le et al., 2003; Li et al., 2003). *PIR*, *ATNAP125* and *DIS2* (*ARPC2*) were expressed at similar levels in the major organs, several of which lacked trichomes (Fig. 3).

The WAVE complex assembles via a series of binary interactions between complex subunits (Gautreau et al., 2004; Innocenti et al., 2004). We tested the ability of PIR to directly bind ATNAP125. In pull-down assays employing purified full-length recombinant proteins, GST-tagged PIR interacted with ATNAP125 (Fig. 4A, upper lane 2). The binding experiments were repeated three times with two different protein preparations, and under these reaction conditions, 4±1% of ATNAP125 was bound by the GST-PIR beads. No significant binding was detected with the GST control beads (Fig. 4A, upper lane 4). The observed PIR-ATNAP125 interaction was not due to non-specific binding of PIR to the HIS-tag of ATNAP125 because GST-PIR-beads did not interact with a HIS-tagged version of an unrelated 140 kDa protein (Fig. 4A, lower, lanes 1 to 3).

The two-hybrid assay has been used successfully to assay interactions between *C. elegans* GEX-2 (SRA1) and GEX-3 (NAP125) (Soto et al., 2002). Therefore, we used it to test the specificity of the interactions between SRA1 and NAP125 proteins from *Arabidopsis* and humans. We confirmed the

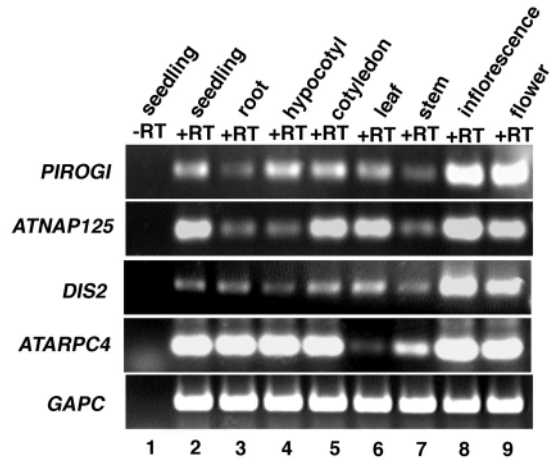


Fig. 3. Expression patterns of *PIR*, *ATNAP125* and ARP2/3 subunit genes in major organs. Lane 1, no reverse transcriptase (–RT) in 5 DAG seedling; lane 2, plus (+) RT in 5 DAG seedling; lane 3, 5 DAG root (+RT); lane 4, 5 DAG hypocotyl (+RT); lane 5, 5 DAG cotyledon (+RT); lane 6, 15 DAG leaf (+RT); lane 7, stem (+RT); lane 8, inflorescence (+RT); lane 9, flower (+RT). No RT controls were conducted on all RNA samples, but the data are shown only for the seedling RNA sample.

known interaction between the human SRA1 and NAP125 (Fig. 4B). We also detected a direct interaction between *Arabidopsis PIR* and ATNAP125. Yeast strains that harbored *PIR* bait (pDS32PIR) and ATNAP125 prey (pDS22ATNAP) plasmids were able to grow on His[−] media and activated the β-gal reporter gene more than 14-fold relative to controls (Fig. 4B). We next tested the ability of human SRA1 to interact with ATNAP125. Surprisingly, the animal-plant pair of fusion proteins strongly activated the β-gal reporter gene relative to controls. We then tested the ability of the human protein to provide PIR function in *Arabidopsis*. When overexpressed in the *pir-3*-null mutant background, human *SRA1* yielded symmetrical three-branched trichomes (Fig. 4C) and adherent cotyledon pavement cells (data not shown) that were indistinguishable from the wild type. Overexpression of human *SRA1* in the wild-type background did not cause observable defects.

If PIR and human SRA1 functions are truly interchangeable, one would expect to detect conserved interactions with RHO-family GTPases. SRA1 interacts specifically with the small GTPase Rac1 (Kobayashi et al., 1998), and we were able to use the two-hybrid assay to confirm this interaction (Fig. 5A). We next tested the ability of PIR to interact with *Arabidopsis* RHO-family GTPases. *Arabidopsis* encodes 11 RHO-family GTPases that are members of a plant specific family of small GTPases termed ROPs (Rho of plants) (Christensen et al., 2003; Vernoud et al., 2003). *ATROP2* is expressed in leaves and overexpression of dominant mutant forms of this isoform causes epidermal shape defects (Fu et al., 2002). Therefore, we tested whether or not *Arabidopsis PIR* could interact with ATROP2, ATROP8 as a control, human RAC1 and human CDC42 in a two-hybrid assay. In these experiments, each of the small GTPases were expressed at similar levels and did not activate the *HIS3* or β-Gal reporter genes when tested in isolation (data not shown). However, when ATROP2 was co-

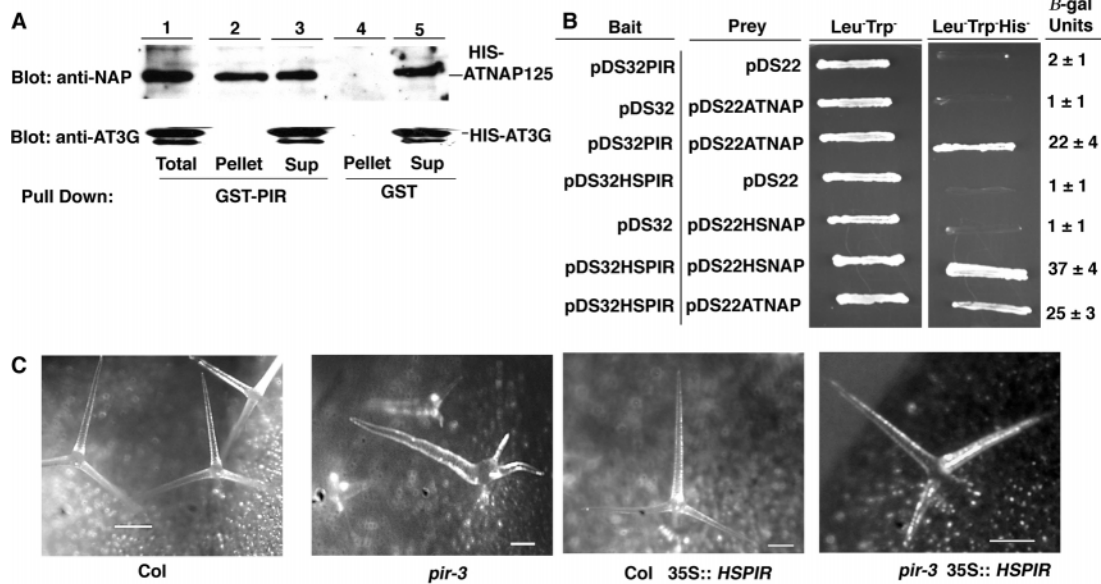
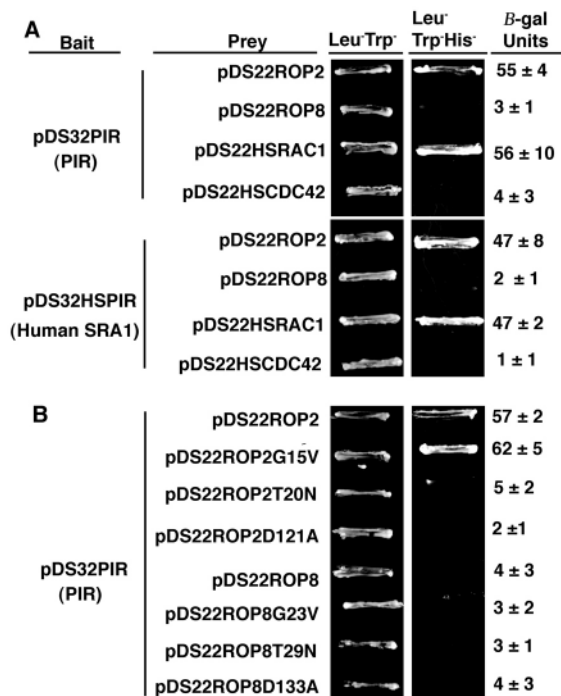


Fig. 4. *Arabidopsis* PIR and human SRA1 have interchangeable in vivo functions and interactions with ATNAP125. (A) Direct interaction of recombinant PIR and ATNAP125 in a GST-pull-down assay. (Top) Lanes 1-5, fractions probed with anti-ATNAP antibody; (bottom) same fractions probed with control antibody anti-AT3G. Lane 1, 5% of total binding reaction; lane 2, GST-PIR bead bound pellet fraction; lane 3, GST-PIR bead unbound; lane 4, GST bead bound; lane 5, GST bead unbound. (B) PIR and human SRA1 interact with ATNAP125 in a yeast two-hybrid assay. The bait and prey plasmids that were co-transformed into yeast are defined to the left of the corresponding yeast patches and β -galactosidase assay results. pDS32PIR, full-length PIR; pDS32HSPiR, full-length human SRA1; pDS22ATNAP, full-length ATNAP125; pDS22HSNAP, full-length human NAP125. (C) Overexpression of human SRA1 can suppress *pir-3* trichome distortion. Left to right: Col mature trichome; *pir-3* mature trichome; mature trichome on a Col plant that harbors a human SRA1 overexpression construct; mature trichome on a *pir-3* plant that harbors a human SRA1 overexpression construct. Scale bars: 100 μ m.

expressed with PIR a strong interaction was detected (Fig. 5A). No interactions were detected between PIR and ATROP8 or human CDC42. In another set of inter-kingdom two-hybrid assays, PIR displayed a strong interaction with RAC1 and human SRA1 interacted with ATROP2 (Fig. 5A).



To determine if the interaction of PIR with ATROP2 was sensitive to the nucleotide status of ATROP2, we made constitutively active mutant forms of the protein that are predicted to stabilize the GTP-bound form of the protein (ROP2G15V) and dominant-negative forms of the GTPase that either reduce the affinity of the GTPase for GTP (ROPT20N) or guanine nucleotides in general (ROP2D121A). Putative ATROP effectors, such as the ROP interacting CRIB motif (RIC) proteins (Wu et al., 2001) bind with selectivity to the ROPG15V class of mutants. PIR retained a strong interaction with the constitutively active form of ATROP2, but failed to interact with either of the dominant-negative forms of ATROP2 that were tested (Fig. 5B). Mutation of ATROP8 to an analogous constitutively active form (ROP8G23V) did not convert it to a PIR-binding protein (Fig. 5B).

Depending on the cell type, loss of SRA1 function can lead to either increased levels of actin filaments and gain-of-function actin-based phenotypes (Blagg et al., 2003), or to reduced amounts of cortical actin at the leading edge of migrating cells and a failure to generate normal lamellipodia (Kunda et al., 2003; Rogers et al., 2003). Therefore, we wanted

Fig. 5. *Arabidopsis* PIR and human SRA1 have similar RHO-family GTPase binding activities. (A) PIR and human SRA1 bind interchangeably to plant and animal RHO-family GTPases in the yeast two-hybrid assay. The bait and prey plasmids co-transformed into yeast are listed to the left of the corresponding patches and β -galactosidase assay results. (B) PIR shows nucleotide-selectivity for interaction with ROP2 in yeast two-hybrid system. The bait and prey plasmids co-transformed into yeast are described to the left as in A.

to determine if the actin cytoskeleton in stage 4 *pir* trichomes differed from that of the wild-type and *dis2* (*arp2*). Because changes in branch morphology during stage 4 is an early and obvious indicator of actin and ARP2/3 function, we concentrated our actin localization efforts on this stage of development. Stage 4 wild-type (Fig. 6A), *dis2* (*arp2*) (Fig. 6D) and *pir* (Fig. 6G) trichomes had an intricate, interconnected actin cytoskeleton that was present throughout the stalks and developing branches. Wild-type (Fig. 6B), *dis2* (Fig. 6E) and *pir* (Fig. 6H) stage 4 branches have a dense reticulate network of cortical actin filaments. Given the complexity of cortical actin organization and the lack of a specific marker for ARP2/3 subunits, we have not detected clear phenotypes in this region of the cell. Wild-type stage 4 trichomes contain a dense population of core bundles, and in all observations ($n=10$), many of the core bundles terminated within 1 μm of the apical plasma membrane. Fig. 6C contains a representative image. Fifty-three percent of *pir* early stage 4 branches ($n=15$) contained a dense population of core cytoplasmic bundles that were aligned with the long axis of the branch (Fig. 6I). In 29% of the stage 4 *pir* branches analyzed ($n=15$), the bundles terminated at least 2 μm distal to the apical plasma membrane (Fig. 6I). At the same time, the apical surface of the *pir* branches tended to be prematurely refined to a sharp tip. Therefore, we do not know the cause-and-effect relationships between the core bundles and the branch tip morphology in *pir* trichomes. Ninety-one percent ($n=11$) of *dis2* trichomes lacked a population of core bundles (Fig. 6F).

Most of the cell volume is generated during stage 5 (Szymanski et al., 1999). During early stage 5 wild-type cells contained many cortical and core cytoplasmic actin filaments along the length of the branch. These filaments and/or bundles adopted a loose alignment with the long axis of the branch (Fig. 7A). The core cytoplasm of similarly staged *dis2* branches was largely devoid of aligned actin bundles (Fig. 7B), but elsewhere in the cell there were many filaments or fine bundles. The organization of actin bundles in early stage 5 *pir* branches was variable, ~50% ($n=10$) of *pir* branches from 30-75 μm in length had a core cytoplasm that lacked a population of clearly aligned bundles (Fig. 7C). In all *dis2* ($n=11$) and *pir* branches of this class, the cytoplasm was dominated by large vacuole compartments that lacked the background fluorescence of the cytosol. An approximately equal fraction of early stage 5 *pir* branches had a dense population of core bundles (Fig. 7D) that resembled those of the wild type. Despite the presence of core bundles in many developing *pir* branches, all were swollen to some degree, and few attained a final length that equaled the mean length of mature wild-type trichomes (Table 1).

As previously reported for *dis1* (*arp3*) (Le et al., 2003) and *dis2* (*arp2*) (El-Assal et al., 2004a), we did not detect quantitative differences between *pir* and wild-type stage 3/4 trichomes in the relative amounts of core actin filaments in early stage 4 cells (Fig. 6J). Late stage 4 *dis2* trichomes have significantly reduced relative amounts of core actin bundles (El-Assal et al., 2004a). Although the mean relative ratio of core:total cytoplasmic F-actin was not significantly different between *pir* and wild-type stage 4/5 branches, there appeared to be a distinct subpopulation with reduced relative F-actin levels (Fig. 6J). The mean core:total ratio for one group clearly fell within the 95% confidence interval of the wild-type value, while another subset of similarly staged branches had reduced

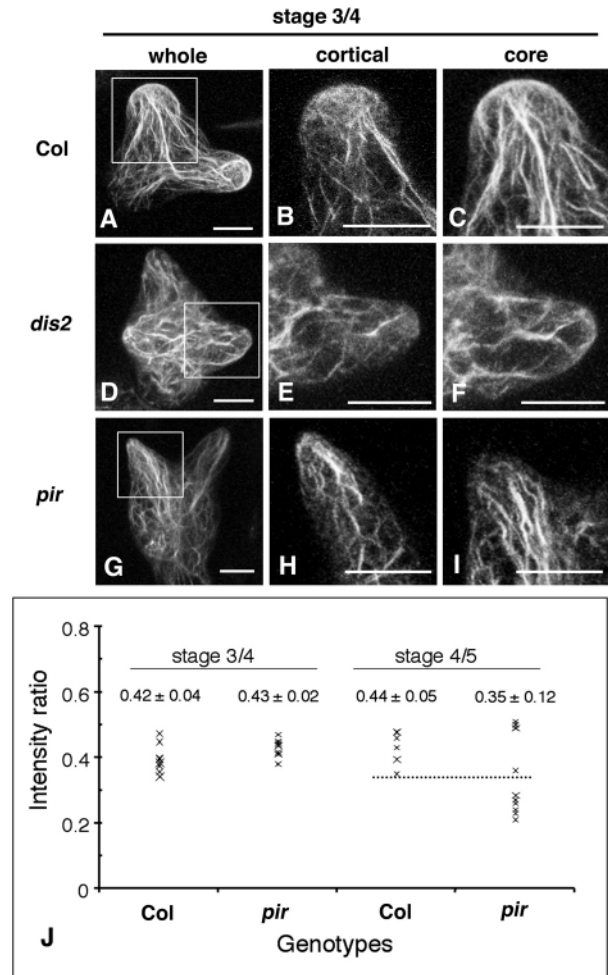


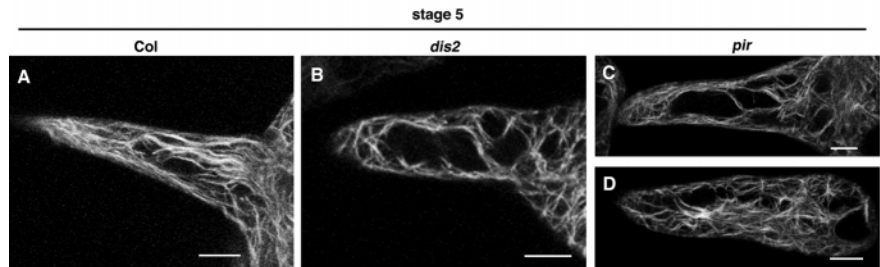
Fig. 6. Localization and quantification of actin filaments in whole mounted wild-type (Col), *dis2* and *pir* stage 4 trichomes. (A-C) Wild-type. (D-F) *dis2-1*. (G-I) *pir-3*. (A,D,G) Maximum projection of whole-cell F-actin signals in stage 4 trichomes. (B,E,H) Maximum projection of signals from cortical actin filaments (within 2.5 μm of the plasma membrane) in the same branches of A, D and G, respectively. (C,F,I) Maximum projection of signals from actin filaments in the core branch cytoplasm. (J) Mean ratios \pm s.d. of core cytoplasmic to total cytoplasmic actin filament signals in stage 3/4 and stage 4/5 branches from 5-10 branches. Broken line indicates the lower limit of the 95% confidence level of the mean ratio for wild-type stage 4/5 trichomes. Scale bars: 10 μm .

core:total F-actin ratios that did not differ from those measured for ARP2/3 subunit mutants (El-Assal et al., 2004a; Le et al., 2003).

Discussion

The 'distorted group' of trichome mutants defines approximately eight loci that are required for actin-dependent cell shape transitions in trichomes (Hulskamp et al., 1994). A subset of the genes in this pathway encode homologs of ARP2/3 subunits. This paper extends our knowledge, and demonstrates that *PIR* encodes a homolog of the WAVE complex subunit SRA1. Three lines of evidence allow us to

Fig. 7. Organization of actin filaments in wild-type (Col), *dis2* and *pir-3* early stage 5 trichomes. Trichomes belonging to this stage were identified by a pointed tip morphology, the absence of papillae, a cell height of at least 40 μm , and a branch length between 30 and 75 μm . Each image is a projection of planes that correspond to the core branch cytoplasm. (A) Wild-type. (B) *dis2-1*. (C,D) *pir-3*. Scale bars: 10 μm .



conclude that we correctly identified the *PIR* gene. First, four independent *pir* alleles harbor mutations in the *PIR* gene. Second, the T-DNA insertion line SALK_106757 prematurely terminates *PIR* transcription, causes trichome distortion in homozygous lines and is allelic to *pir*. Third, we could rescue the *pir* phenotype by overexpressing the wild-type gene with the strong viral 35S promoter. These results are important because they prove the general relevance of the distorted mutants to study ARP2/3 function from signaling input to cell shape output.

The only known function of vertebrate SRA1 is to regulate ARP2/3-dependent cell motility. Several facts support the idea that *PIR* and ARP2/3 subunit genes have related functions. First, mutation of *PIR* and ARP2/3 subunit-like genes causes identical trichome distortion, epidermal cell-cell adhesion and reduced fresh weight phenotypes. Second, although the actin bundle phenotypes of *pir* and ARP2/3 subunit mutants are distinct at early stages, in both mutant classes there is a failure to maintain core actin bundles in elongating branches (Figs 6, 7). Third, *PIR* interacts with ATNAP125 and active forms of ATROP2 (Figs 4, 5); these binding interactions are expected for a SRA1 family member. Fourth, overexpression of human SRA1 completely rescues the *pir* trichome phenotypes. The simplest explanation of the *pir* rescue result is that *Arabidopsis* and human SRA1 function interchangeably by linking small GTPase inputs to altered ARP2/3 activity. Last, *PIR*, *ATNAP125* and ARP2/3 subunit-like genes such as *DIS2* (*ARPC2A*) are expressed at similar relative levels in all of the major organs tested (Fig. 3).

If *PIR* directly regulates *Arabidopsis* ARP2/3, then the similar cell shape and actin phenotypes of *PIR* and ARP2/3 subunit mutants suggest that *PIR* positively regulates ARP2/3. These results are consistent with those obtained by using RNA interference of *SRA1* in cultured insect cells (Kunda et al., 2003; Rogers et al., 2003). A positive role for SRA1 in signaling to ARP2/3 is also suggested by the ability of activated Rac1 to relocalize fully assembled and active WAVE complex to the leading of stimulated cells (Innocenti et al., 2004; Steffen et al., 2004). Other biochemical (Eden et al., 2002) and genetic (Blagg et al., 2003) data suggest that SRA1 negatively regulates ARP2/3. The reasons for these discrepancies are not known, but they could, in part, be explained if cell types differ, either with respect to functional redundancy at the level of F-actin nucleation, or in their ability to accumulate or localize WAVE-like proteins in a *SRA1*-independent manner.

Although plant and human *SRA1* homologs are functionally interchangeable, plant development is less sensitive to removal of its function. The subtle *PIR*-null phenotypes differ greatly from the embryonic lethality and severe morphological

defects that are caused by null *SRA1* alleles in *Drosophila* (Schenck et al., 2001) and *C. elegans* (Soto et al., 2002). Mutations in several *Arabidopsis* ARP2/3 subunit-like genes have similar mild-effects on whole plant development. These results suggest that ARP2/3-dependent nucleation has important but non-essential functions in *Arabidopsis*. It is generally accepted that plants cells use turgor force to push the plasma membrane against the rigid cell wall and drive cell expansion: therefore, the mechanical energy of ARP2/3-dependent nucleation may be used for other functions (see Vidali and Hepler, 2001; Wasteneys and Galway, 2003). In plant cells, the dynamics of the tonoplast membrane is cytochalasin D-sensitive (Uemura et al., 2002); in *S. cerevisiae*, vacuole biogenesis is ARP2/3-dependent (Eitzen et al., 2002). The vacuole morphology (Mathur et al., 2003a) and positioning defects in ARP2/3 subunit mutants (El-Assal et al., 2004a; Le et al., 2003) and *pir* (Fig. 6J and Fig. 7C) imply a role for *Arabidopsis* ARP2/3 in vacuole-based functions. More-detailed information on ARP2/3 function in the context of membrane trafficking and organelle motility is needed to define the cellular function of ARP2/3 in plants and to understand why there is so much variability in the extent to which different cell types rely on ARP2/3 function. For example, is the apparent unimportance of *PIR* and ARP2/3 for the tip growth of pollen tubes, which has a strict actin-dependence (Gibbon et al., 1999), owing to cell-type specific strategies for actin-dependent growth or to differences in the extent to which pathways leading to actin filament nucleation are functionally redundant? Perhaps different plant cell types use combinations of FORMIN (Cvrckova, 2000; Deeks et al., 2002) and ARP2/3 activities to fine tune actin filament nucleation and morphogenesis.

At a molecular level, the protein-protein interactions of the human and plant SRA1 homologs are remarkably similar. In non-plant cells, the molecular function of SRA1 is to link Rac1 signaling with WAVE-dependent regulation of ARP2/3 (Steffen et al., 2004). *PIR* interacts with RHO-family GTPases, and binds to ATROP2 with some degree of isoform and nucleotide selectivity (Fig. 5A,B). NAP125 is an essential subunit of the WAVE complex (Bogdan and Klambt, 2003) that directly interacts with SRA1 (Soto et al., 2002). Using full-length recombinant proteins, we detected a direct interaction between *PIR* and ATNAP125 in both the yeast two-hybrid and GST-pull down assays (Fig. 4). Therefore *PIR* contains the functional domains that are known to mediate WAVE complex signaling. Small N- or C-terminal truncations of *C. elegans* GEX-2 (*SRA1*) eliminate its ability to bind GEX-3 (*NAP125*) (Soto et al., 2002). If the *PIR*-ATNAP125 interaction is similarly constrained, the similar phenotypes of the *pir* null alleles and those that encode C-terminal truncations (Fig. 2B)

could reflect the inability of any of the mutant proteins to bind ATNAP125.

The interchangeable RHO-GTPase binding and in vivo functions of *Arabidopsis* and human SRA1 homologs suggest that during multicellular development there have been extreme structural constraints on this particular RHO-GTPase switch. There are substantial in vivo data that support a Rac1-dependent pathway of SRA1 signaling to ARP2/3. RNA interference of three Rac1-like functions in cultured insect cells cause phenotypes that are identical to those of SRA1 loss of function (Kunda et al., 2003). Activation of Rac1-signaling pathways in cultured cells relocalizes SRA1 and other WAVE complex subunits (Steffen et al., 2004) to locations in the cell that are defined by ARP2/3-dependent nucleation (Svitkina and Borisy, 1999). A similar regulatory pathway in *Arabidopsis* may include PIR as an ATROP2 effector. PIR specifically binds ATROP2 both with isoform specificity and with selectivity for active forms of the small GTPase (Fig. 5). Some degree of redundancy at the level of PIR-ROP interaction is expected in *Arabidopsis*, because overexpression of dominant-negative or constitutively active forms of ATROP2 within the strong viral 35S-promoter does not cause trichome distortion (Fu et al., 2002).

The protein-protein interaction data and the interchangeable functions of human and *Arabidopsis* SRA1 homologs are consistent with the idea that PIR encodes a subunit of the WAVE complex. However, the composition of the putative *Arabidopsis* WAVE complex is unknown. Of the five known WAVE subunits (Eden et al., 2002), only SRA1-, NAP125- and HSPC300-like genes are easily identified in sequence databases. With respect to ATNAP125, we recently learned the 'distorted group' gene *GNARLED* corresponds to this gene, and that human NAP125 functions interchangeably with the plant homolog (El-Assal et al., 2004b). *Arabidopsis* encodes a homolog of human HSPC300 that we termed *ATBRK1*. *ATBRK1* is expressed in *Arabidopsis*, but has no known function. In maize, *BRK1* is required for the crenulation of leaf epidermal cells (Frank and Smith, 2002). The plant protein sequence database does not encode an obvious ortholog of the ARP2/3 activator WAVE or the WAVE complex subunit ABI2 (ABL-Interaction 2) (Eden et al., 2002). The N-terminal domains of WAVE and ABI2 may mediate assembly of both subunits into the WAVE complex (Innocenti et al., 2004). *Arabidopsis* encodes small gene families with homology that is restricted to the corresponding N-terminal domains of WAVE and ABI2 (D.B.S., unpublished). *Arabidopsis* WAVE- and ABI2-like subunits may have retained the domains needed for the assembly of an analogous plant complex.

Conclusion

The 'distorted group' of trichome mutants provide a powerful genetic entry point into signaling to ARP2/3, morphogenesis and multi-cellular development. Specifically, the apex of stage 4 branches will be a useful experimental testing ground to understand how cortical microtubules and actin filaments control the dynamics of cytoplasmic organization and polarized growth. The 'distorted group' appears to define a class of genes that specifically affect the activity and assembly of ARP2/3. Given the diversity of the cell shape and adhesion defects of the distorted mutants and the known functions of ARP2/3 in membrane protrusion, motility and endocytosis, we

expect 'distorted group' genes to have multiple functions in the cell. It has been proposed that *Arabidopsis* ARP2/3 generates actin filament networks that are required for organelle and vesicle transport (Li et al., 2003; Mathur et al., 2003a; Mathur et al., 2003b). In our hands, the clearest actin phenotype of the ARP2/3 subunit mutants is the failure to populate the branch cytoplasm with aligned actin filaments and bundles. In this context, potential functions of PIR, ARP2/3 and core actin bundles include membrane trafficking to the vacuole and/or the physical interactions with expanding central vacuole. Actin filament and/or bundle interactions with the vacuole may serve the purpose of mechanically excluding the expanding central vacuole from regions of the cell that grow persistently or to alter the dynamics of the tonoplast. If true, one expects the apical dome of stage 4 branches to be a busy site for ROP signaling, PIR-dependent activation of ARP2/3 and the generation of aligned actin bundles. It will be interesting to find out how directly the rules of PIR signaling and morphogenesis transfer from trichomes to other cell types and species.

Note added in proof

While this work was under review, related work on the cloning of *GNARLED* was published online (2 July 2004) (El-Assal et al., 2004b).

We are very grateful to the Purdue Motility Group for helpful discussions along the way. Thanks to Gregore Koliantz for coordinating the mutant screens, to Chris Staiger and Traci Matsumoto for the generous gift of pATPOP140, to Johnathon Chernoff for the gift of the human Cdc42 and Rac1 expression clones, to Zhenbiao Yang for the ATROP2 and ATROP8 expression clones, and to Martin Huelskamp for sending a *klunker* allele for complementation tests. We are indebted to the *Arabidopsis* stock center for many key seed and DNA reagents. Thanks also to the Purdue Genomics Center and Phillip SanMiguel for DNA sequencing. This work was supported by National Science Foundation grant 0110817-IBN, by a Department of Energy grant DE-FG02-02ER15357 and by a Purdue Agricultural Research Program fellowship to D.B.S.

References

- Alonso, J. M., Stepanova, A. N., Leisse, T. J., Kim, C. J., Chen, H., Shinn, P., Stevenson, D. K., Zimmerman, J., Barajas, P., Cheuk, R. et al. (2003). Genome-wide insertional mutagenesis of *Arabidopsis thaliana*. *Science* **301**, 653-657.
- Amann, K. and Pollard, T. D. (2001). Direct real-time observation of actin filament branching mediated by Arp 2/3 complex using total internal reflection fluorescence microscopy. *Proc. Natl. Acad. Sci. USA* **98**, 15009-15013.
- Assaad, F. F. (2001). Of weeds and men, what genomes teach us about plant cell biology. *Curr. Opin. Plant Biol.* **4**, 478-487.
- Ausubel, F. M., Brent, R., Kingston, R. E., Moore, D. D., Seidman, J. G., Smith, J. A. and Struhl, K. (1994). *Current protocols in molecular biology*. New York, NY: John Wiley & Sons.
- Baluska, F., Salaj, J., Mathur, J., Braun, M., Jasper, F., Samaj, J., Chua, N. H., Barlow, P. W. and Volkmann, D. (2000). Root hair formation, F-actin-dependent tip growth is initiated by local assembly of profilin-supported F-actin meshworks accumulated within expansin-enriched bulges. *Dev. Biol.* **227**, 618-632.
- Beilstein, M. and Szymanski, D. (2003). Cytoskeletal requirements during *Arabidopsis* trichome development. In *The Plant Cytoskeleton in Cell Differentiation and Development* (ed. P. Hussey), pp. 265-289. Oxford, UK: Blackwell.
- Blagg, S. L. and Insall, R. H. (2004). Solving the WAVE function. *Nat. Cell Biol.* **6**, 279-281.

- Blagg, S. L., Stewart, M., Sambles, C. and Insall, R. H. (2003). PIR121 regulates pseudopod dynamics and SCAR activity in *Dictyostelium*. *Curr. Biol.* **13**, 1480-1487.
- Blanchoin, L., Amann, K. J., Higgs, H. N., Marchand, J. B., Kaiser, D. A. and Pollard, T. D. (2000). Direct observation of dendritic actin filament networks nucleated by Arp2/3 complex and WASP/Scar proteins. *Nature* **404**, 1007-1011.
- Bogdan, S. and Klambt, C. (2003). Kette regulates actin dynamics and genetically interacts with Wave and Wasp. *Development* **130**, 4427-4437.
- Christensen, T. M., Vejlupekova, Z., Sharma, Y. K., Arthur, K. M., Spatafora, J. W., Albright, C. A., Meeley, R. B., Duvick, J. P., Quatrano, R. and Fowler, J. E. (2003). Conserved subgroups and developmental regulation of the monocot ROP gene family. *Plant Physiol.* **133**, 1791-1808.
- Clough, S. and Bent, A. (1998). Floral dip, a simplified method for *Arabidopsis thaliana* transformation. *Plant J.* **16**, 735-743.
- Cvrckova, F. (2000). Are plant formins integral membrane proteins? *Genome Biol.* **1**, research001.1-001.7.
- Deeks, M. J., Hussey, P. J. and Davies, B. (2002). Formins, intermediates in signal-transduction cascades that affect cytoskeletal reorganization. *Trends Plant Sci.* **7**, 492-498.
- Eden, S., Rohatgi, R., Podtelejnikov, A. V., Mann, M. and Kirschner, M. (2002). Mechanism of regulation of WAVE1-induced actin nucleation by Rac1 and Nck. *Nature* **418**, 790-793.
- Eitzen, G., Wang, L., Thorngren, N. and Wickner, W. (2002). Remodeling of organelle-bound actin is required for yeast vacuole fusion. *J. Cell Biol.* **158**, 669-679.
- El-Assal, S. E., Le, J., Basu, D., Mallery, E. L. and Szymanski, D. B. (2004a). *DISTORTED2* encodes an ARPC2 subunit of the putative Arabidopsis ARP2/3 complex. *Plant J.* **38**, 526-538.
- El-Assal, S. E., Le, J., Basu, D., Mallery, E. L. and Szymanski, D. B. (2004b). Arabidopsis *GNARLED* encodes a NAP125 homologue that positively regulates ARP2/3. *Curr. Biol.* (in press)
- Frank, M. J. and Smith, L. G. (2002). A small, novel protein highly conserved in plants and animals promotes the polarized growth and division of maize leaf epidermal cells. *Curr. Biol.* **12**, 849-853.
- Fu, Y., Li, H. and Yang, Z. (2002). The ROP2 GTPase controls the formation of cortical fine F-actin and the early phase of directional cell expansion during *Arabidopsis* organogenesis. *Plant Cell* **14**, 777-794.
- Gautreau, A., Ho, H. Y., Steen, H., Gygi, S. P. and Kirschner, M. W. (2004). Purification and architecture of the ubiquitous Wave complex. *Proc. Natl. Acad. Sci. USA* **101**, 4379-4383.
- Gibbon, B. C., Kovar, D. R. and Staiger, C. J. (1999). Latrunculin B has different effects on pollen germination and tube growth. *Plant Cell* **11**, 2349-2363.
- Hulkamp, M., Misra, S. and Jürgens, G. (1994). Genetic dissection of trichome cell development in *Arabidopsis*. *Cell* **76**, 555-566.
- Innocenti, M., Zucconi, A., Disanza, A., Frittoli, E., Arecas, L., Steffen, A., Stradal, T. E., di Fiore, P. P., Carlier, M. and Scita, G. (2004). Abi1 is essential for the formation and activation of a WAVE2 signaling complex mediating Rac-dependent actin remodeling. *Nat. Cell Biol.* **6**, 319-327.
- Johnson, H. B. (1975). Plant pubescence, an ecological perspective. *Bot. Rev.* **41**, 233-258.
- Kobayashi, K., Kuroda, S., Fukata, M., Nakamura, T., Nagase, T., Nomura, N., Matsuura, Y., Yoshida-Kubomura, N., Iwamatsu, A. and Kaibuchi, K. (1998). p140Sra-1 (specifically Rac1-associated protein) is a novel specific target for Rac1 small GTPase. *J. Biol. Chem.* **273**, 291-295.
- Kunda, P., Craig, G., Dominguez, V. and Baum, B. (2003). Abi, Sra1, and Kette control the stability and localization of SCAR/WAVE to regulate the formation of actin-based protrusions. *Curr. Biol.* **13**, 1867-1875.
- Le, J., El-Assal, S. E., Basu, D., Saad, M. E. and Szymanski, D. B. (2003). Requirements for *Arabidopsis* ATARP2 and ATARP3 during epidermal development. *Curr. Biol.* **13**, 1341-1347.
- Li, S., Blanchoin, L., Yang, Z. and Lord, E. M. (2003). The putative Arabidopsis Arp2/3 complex controls leaf cell morphogenesis. *Plant Physiol.* **132**, 2034-2044.
- Machesky, L. and Insall, R. (1998). Scar1 and the related Wiskott-Aldrich syndrome protein, WASP, regulate the actin cytoskeleton through the Arp 2/3 complex. *Curr. Biol.* **8**, 1347-1356.
- Machesky, L., Mullins, R., Higgs, H., Kaiser, D., Blanchoin, L. R. M., Hall, M. and Pollard, T. (1999). Scar, a WASP-related protein, activates nucleation of actin filaments by the Arp 2/3 complex. *Proc. Natl. Acad. Sci. USA* **96**, 3739-3744.
- Mathur, J. and Hulkamp, M. (2002). Microtubules and microfilaments in cell morphogenesis in higher plants. *Curr. Biol.* **12**, R669-R676.
- Mathur, J., Spielhofer, P., Kost, B. and Chua, N. (1999). The actin cytoskeleton is required to elaborate and maintain spatial patterning during trichome cell morphogenesis in *Arabidopsis thaliana*. *Development* **126**, 5559-5568.
- Mathur, J., Mathur, N., Kernebeck, B. and Hulkamp, M. (2003a). Mutations in actin-related proteins 2 and 3 affect cell shape development in *Arabidopsis*. *Plant Cell* **15**, 1632-1645.
- Mathur, J., Mathur, N., Kirik, V., Kernebeck, B., Srinivas, B. P. and Hulkamp, M. (2003b). *Arabidopsis* *CROOKED* encodes for the smallest subunit of the ARP2/3 complex and controls cell shape by region specific fine F-actin formation. *Development* **130**, 3137-3146.
- Pollard, T. and Beltzner, C. (2002). Structure and function of the Arp 2/3 complex. *Curr. Opin. Cell Biol.* **12**, 768-774.
- Rogers, S. L., Wiedemann, U., Stuurman, N. and Vale, R. D. (2003). Molecular requirements for actin-based lamella formation in *Drosophila* S2 cells. *J. Cell Biol.* **162**, 1079-1088.
- Rohatgi, R., Ho, H. H. and Kirschner, M. W. (2000). Mechanism of N-WASP activation by CDC42 and phosphatidylinositol 4,5-bisphosphate. *J. Cell Biol.* **150**, 1299-1310.
- Saller, E., Tom, E., Brunori, M., Otter, M., Estreicher, A., Mack, D. H. and Iggo, R. (1999). Increased apoptosis induction by 121F mutant p53. *EMBO J.* **18**, 4424-4437.
- Sawa, M., Suetsugu, S., Sugimoto, A., Miki, H., Yamamoto, K. and Takenawa, T. (2003). Essential role of the *C. elegans* Arp2/3 complex in cell migration during ventral enclosure. *J. Cell Sci.* **116**, 1505-1518.
- Schafer, D. A. (2002). Coupling actin dynamics and membrane dynamics during endocytosis. *Curr. Opin. Cell Biol.* **14**, 76-81.
- Schenck, A., Bardoni, B., Moro, A., Bagni, C. and Mandel, J.-L. (2001). A highly conserved protein family interacting with the fragile X mental retardation protein (FMRP) and displaying selective interactions with FMRP-related proteins FXR1P and FXR2P. *Proc. Natl. Acad. Sci. USA* **98**, 8844-8849.
- Schwab, B., Mathur, J., Saedler, R., Schwarz, H., Frey, B., Scheidegger, C. and Hulkamp, M. (2003). Regulation of cell expansion by the *DISTORTED* genes in *Arabidopsis thaliana*, actin controls the spatial organization of microtubules. *Mol. Genet. Genomics* **269**, 350-360.
- Soto, M. C., Qadota, H., Kasuya, K., Inoue, M., Tsuboi, D., Mello, C. C. and Kaibuchi, K. (2002). The GEX-2 and GEX-3 proteins are required for tissue morphogenesis and cell migrations in *C. elegans*. *Genes Dev.* **16**, 620-632.
- Staiger, C. J. and Hussey, P. J. (2003). Actin and actin-modulating proteins. In *The Plant Cytoskeleton in Cell Differentiation and Development* (ed. P. Hussey), pp. 32-80. Oxford, UK: Blackwell.
- Steffen, A., Rottner, K., Ehinger, J., Innocenti, M., Scita, G., Wehland, J. and Stradal, T. E. (2004). Sra-1 and Nap1 link Rac to actin assembly driving lamellipodia formation. *EMBO J.* **23**, 749-759.
- Stevenson, V., Hudson, A., Cooley, L. and Theurkauf, W. (2002). Arp 2/3-dependent pseudocleavage furrow assembly in syncytial *Drosophila* embryos. *Curr. Biol.* **12**, 705-711.
- Svitkina, T. and Borisy, G. (1999). Arp2/3 and actin depolymerizing factor/cofilin in dendritic organization and treadmill of actin filament array in Lamellipodia. *J. Cell Biol.* **145**, 1009-1026.
- Svitkina, T. M., Bulanova, E. A., Chaga, O. Y., Vignjevic, D. M., Kojima, S., Vasiliev, J. M. and Borisy, G. G. (2003). Mechanism of filopodia initiation by reorganization of a dendritic network. *J. Cell Biol.* **160**, 409-421.
- Szymanski, D. B. (2001). *Arabidopsis* trichome morphogenesis, a genetic approach to studying cytoskeletal function. *J. Plant Growth Regul.* **20**, 131-140.
- Szymanski, D. B., Marks, M. D. and Wick, S. M. (1999). Organized F-actin is essential for normal trichome morphogenesis in *Arabidopsis*. *Plant Cell* **11**, 2331-2347.
- Uemura, T., Yoshimura, S. H., Takeyasu, K. and Sato, M. H. (2002). Vacuolar membrane dynamics revealed by GFP-AtVam3 fusion protein. *Genes Cells* **7**, 743-753.
- Vernoud, V., Horton, A. C., Yang, Z. and Nielsen, E. (2003). Analysis of the small GTPase gene superfamily of Arabidopsis. *Plant Physiol.* **131**, 1191-1208.
- Vidali, L. and Hepler, P. K. (2001). Actin and pollen tube growth. *Protoplasma* **215**, 64-76.
- Vignjevic, D., Yasar, D., Welch, M. D., Peloquin, J., Svitkina, T. and Borisy,

- G. G.** (2003). Formation of filopodia-like bundles in vitro from a dendritic network. *J. Cell Biol.* **160**, 951-962.
- Wasteney, G. O. and Galway, M. E.** (2003). Remodeling the cytoskeleton for growth and form, an overview with some new views. *Annu. Rev. Plant Biol.* **54**, 691-722.
- Welch, M. D. and Mullins, R. D.** (2002). Cellular control of actin nucleation. *Annu. Rev. Cell Dev. Biol.* **18**, 247-288.
- Winter, D. C., Choe, E. Y. and Li, R.** (1999). Genetic dissection of the budding yeast Arp 2/3 complex, a comparison of the *in vivo* and structural roles of individual subunits. *Proc. Natl. Acad. Sci. USA* **96**, 7288-7293.
- Wu, G.-J., Gaubier-Comella, P., Delseny, M., Grellet, F., van Montagu, M. and Rouze, R.** (1996). Non-canonical introns are at least 10⁹ years old. *Nat. Genet.* **14**, 383-384.
- Wu, G., Gu, Y., Li, S. and Yang, Z.** (2001). A genome-wide analysis of Arabidopsis Rop-interactive CRIB motif-containing proteins that act as Rop GTPase targets. *Plant Cell* **13**, 2841-2856.